

Moderate electron-spin interaction in Fe-intercalated $NbSe_2$

Qiao-Yu Liu(刘乔宇), Jian-Li Bai(白建利), Qing-Xin Dong(董庆新), Li-Bo Zhang(张黎博), Jing-Wen Cheng(程靖雯), Pin-Yu Liu(刘品宇), Cun-Dong Li(李存东), Yu Huang(黄宇), Ying-Rui Sun(孙英睿), Zhi-An Ren(任治安), and Gen-Fu Chen(陈根富)

Citation: Chin. Phys. B, 2025, 34 (**1**): 017502. DOI: 10.1088/1674-1056/ad9735

What follows is a list of articles you may be interested in

Alternating spin splitting of electronic and magnon bands in two-dimensional altermagnetic materials

Qian Wang(王乾), Da-Wei Wu(邬大为), Guang-Hua Guo(郭光华), Meng-Qiu Long(龙孟秋), and Yun-Peng Wang(王云鹏)

Chin. Phys. B, 2024, 33 (**9**): 097507. DOI: 10.1088/1674-1056/ad6425

Relationship between disorder, magnetism and band topology in $Mn(Sb_{1-x}Bi_x)_2Te_4$ single crystals

Ming Xi(席明) and Hechang Lei(雷和畅)

Chin. Phys. B, 2024, 33 (**6**): 067503. DOI: 10.1088/1674-1056/ad3dd8

Spin gap in quasi-one-dimensional *S*=3/2 antiferromagnet $CoTi_2O_5$

Hao-Hang Xu(徐浩航), Qing-Yuan Liu(刘庆元), Chao Xin(辛潮), Qin-Xin Shen(申沁鑫), Jun Luo(罗军), Rui Zhou(周睿), Jin-Guang Cheng(程金光), Jian Liu(刘健), Ling-Ling Tao(陶玲玲), Zhi-Guo Liu(刘志国), Ming-Xue Huo(霍明学), Xian-Jie Wang(王先杰), and Yu Sui(隋郁)

Chin. Phys. B, 2024, 33 (**3**): 037505. DOI: 10.1088/1674-1056/ad1381

Mechanical and magnetocaloric adjustable properties of Fe_3O_4/PET deformed nanoparticle film

Fengguo Fan(范凤国) and Lintong Duan(段林彤)

Chin. Phys. B, 2024, 33 (**3**): 037502. DOI: 10.1088/1674-1056/acf280

Magnetic field enhanced single particle tunneling in MoS_2-superconductor vertical Josephson junction

Wen-Zheng Xu(徐文正), Lai-Xiang Qin(秦来香), Xing-Guo Ye(叶兴国), Fang Lin(林芳), Da-Peng Yu(俞大鹏), Zhi-Min Liao(廖志敏)

Chin. Phys. B, 2020, 29 (**5**): 057502. DOI: 10.1088/1674-1056/ab8209

Moderate electron–spin interaction in Fe-intercalated $NbSe_2$

Qiao-Yu Liu(刘乔宇)[1,2], Jian-Li Bai(白建利)[1,2], Qing-Xin Dong(董庆新)[1,2], Li-Bo Zhang(张黎博)[1,2], Jing-Wen Cheng(程靖雯)[1,2], Pin-Yu Liu(刘品宇)[1,2], Cun-Dong Li(李存东)[1,2], Yu Huang(黄宇)[1,2], Ying-Rui Sun(孙英睿)[1,2], Zhi-An Ren(任治安)[1,2], and Gen-Fu Chen(陈根富)[1,2,3,†]

[1] *Institute of Physics and Beijing National Laboratory for Condensed Matter Physics, Chinese Academy of Sciences, Beijing* 100190, *China*
[2] *School of Physical Sciences, University of Chinese Academy of Sciences, Beijing* 100049, *China*
[3] *Songshan Lake Materials Laboratory, Dongguan* 523808, *China*

(Received 18 October 2024; revised manuscript received 15 November 2024; accepted manuscript online 26 November 2024)

The interaction between charge and spin degrees of freedom has always been the central issue of condensed matter physics, and transition metal dichalcogenides (TMDs) provide an ideal platform to study it benefiting from their highly tunable properties. In this article, the influence of Fe intercalation in $NbSe_2$ was elaborately investigated using a combination of techniques. Magnetic studies have shown that the insertion of Fe atoms induces an antiferromagnetic state in which the easy axis aligns out of the plane. The sign reversal of the magnetoresistance across the Neel temperature can be satisfactorily explained by the moderate interaction between electrons and local spins. The Hall and Seebeck measurements reveal a multi-band nature, and the contribution of various phonon scattering processes is discussed based on the thermal conductivity and specific heat data.

Keywords: transition metal dichalcogenide, intercalation, spin–electron interaction

PACS: 75.50.Ee, 73.50.Lw, 73.43.Qt, 63.20.K–

DOI: 10.1088/1674-1056/ad9735 **CSTR:** 32038.14.CPB.ad9735

1. Introduction

In the last several decades, transition metal dichalcogenides have sparked tremendous research interest due to their novel electronic properties and promising application potential.[1–5] A variety of means have been developed to regulate their properties, such as exfoliating to monolayers, ionic liquid gating and strain engineering, among which the intercalation of guest atoms has been proven to be a powerful method. For instance, the Cu intercalation in 1*T*-$TiSe_2$ suppresses the charge density wave (CDW) state and induces superconductivity,[6] which plausibly results from the increase of Fermi surface dimensionality. In addition, the weakly bonded Cu atoms in the van der Waals gap reduce the thermal conductivity and enhance the thermoelectric performance.[7]

Although remaining nonmagnetic themselves, TMDs can accommodate magnetic atoms in the van der Waals gap and give rise to magnetically ordered states, especially when the intercalation concentration reaches around commensurate values 25% or 33%. For example, $Fe_{0.25}TaS_2$ and $Mn_{0.25}NbS_2$ have been reported to be ferromagnets,[8–10] while $V_{0.33}TaS_2$ and $Fe_{0.33}NbS_2$ behave as antiferromagnets.[11,12] More than the magnetically ordered state, guest magnetic atoms can introduce the Dzyaloshinskii–Moriya interaction if their population locally breaks the spatial inversion symmetry, which stabilizes nontrivial spin textures like magnetic skyrmions.[13] As a consequence of the coupling between conduction electrons and nontrivial spin textures, there emerge fruitful exotic transport behaviors, such as the topological Hall effect in Fe intercalated TaS_2[14] and the negative interlayer magnetoresistance caused by the chiral soliton lattice in $Cr_{0.33}NbS_2$.[15] In the family of TMDs, $NbSe_2$ stands out by virtue of the coexistence of CDW and superconductivity with a relatively high transition temperature. However, the influence of magnetic intercalation on $NbSe_2$ was relatively less paid attention to. Despite that the synthesis of Fe_xNbSe_2 has been previously reported, the research was merely concerned with structures. In anticipation of novel transport behaviors arising from the interaction between guests and hosts, we performed a comprehensive investigation on the transport properties of Fe_xNbSe_2.

2. Experiment details

Single crystalline Fe_xNbSe_2 with the nominal composition of $Fe_{0.33}NbSe_2$ was synthesized by the chemical vapor transport method using polycrystalline samples as the precursor.[16] High-purity Fe powder, Nb powder and Se ingots were weighed in a molar ratio of 0.33 : 1 : 2 and ground thoroughly in an agate mortar under the argon atmosphere of the glove box. Then the mixtures were pressed into pellets and sealed in a quartz tube after evacuating into a high vacuum. The quartz tube was heated to 900 °C for 96 hours and ended up with quenching to the room temperature. Next, the as-grown polycrystalline powders were mixed with an appro-

†Corresponding author. E-mail: gfchen@iphy.ac.cn

© 2025 Chinese Physical Society and IOP Publishing Ltd. All rights, including for text and data mining, AI training, and similar technologies, are reserved.

priate amount of the transport agent iodine and sealed into a quartz tube again. Plate-like shiny crystals with a hexagonal shape were obtained after heating the quartz tube in a two-zone furnace for over two weeks, during which the temperatures of the source zone and the growth zone were kept at 800 °C and 700 °C, respectively. The x-ray diffraction characterization was performed on a PAN-analytical x-ray diffractometer using a Cu target. The chemical compositions were checked with an energy-dispersive x-ray (EDX) spectrometer equipped with a Phenom scanning electron microscope (SEM) operated at 15 kV. The EDX analysis was performed on the fresh surface cleaved from the as-grown crystals. The magnetotransport measurement using a standard four-wire method and specific heat measurement were carried out on a Quantum Design physical properties measurement system (PPMS-9T). The magnetization measurements were conducted on a Quantum Design magnetic properties measurement system (MPMS-7T). The thermoelectric transport measurements were conducted on a home-built platform based on the PPMS-9T dewar which consists of several Keithley source meters and nanovolt meters.

3. Results and discussion

Figures 1(a) and 1(b) show the crystal structure of Fe_xNbSe_2, in which the intercalated Fe atoms constitute ordered Fe superlattices. As shown in Fig. 1(c), the expansion of the c-axis lattice constant is signaled by the shift of diffraction peaks to lower degrees. The EDX analysis indicates that the actual chemical compositions deviate slightly from the nominal compositions, as shown in Fig. 1(d). To avoid confusion, in this study, we call the examined crystal $Fe_{0.33}NbSe_2$ using the nominal composition.

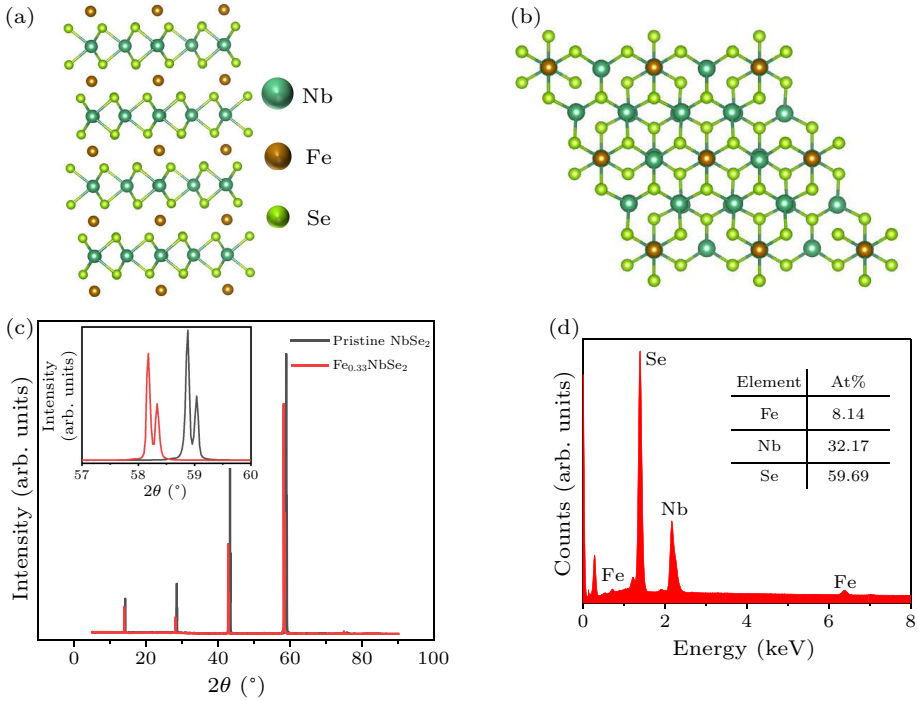


Fig. 1. (a) and (b) The side view and top view of the crystal structure, respectively. The dark green balls, the light green balls and the bronze balls represent Nb atoms, Se atoms and Fe atoms, respectively. (c) The x-ray diffraction pattern of pristine and Fe intercalated $NbSe_2$ single crystals along the $(00l)$ planes, where the black line and the red line correspond to pristine $NbSe_2$ and Fe_xNbSe_2, respectively. The inset shows the enlarged view of their (008) peaks. (d) Element components of the title compound obtained from EDX.

First, in order to investigate the influence of intercalated magnetic atoms on the magnetic properties of the parent compound, the magnetization measurement was conducted. Figure 2(a) shows the temperature dependence of the magnetic susceptibility under an external magnetic field of 1 T applied parallel and perpendicular to the c-axis with both zero field cooling (ZFC) and field cooling (FC) modes respectively. It is shown that the ZFC and FC curves of both directions overlap with each other and exhibit a pronounced cusp-like behavior at $T_N = 160$ K, which is the sign of an antiferromagnetic transition.[17] And it is obvious that the magnetization decreases more rapidly when the magnetic field is parallel to the c-axis once entering the antiferromagnetic state, which indicates that the easy magnetization axis is along the c-axis and resembles the case of $Fe_{0.33}NbS_2$.[12] The susceptibility curves above T_N can be well fitted by the Curie–Weiss law

$$\chi = \frac{C}{T - \theta_W}, \tag{1}$$

where C is the Curie constant and θ_W is the Weiss temperature. As a result, the effective moment μ_{eff} (5.06 μ_B and

4.52 μ_B) and Weiss temperature θ_W (9.9 K and 83.8 K) are derived for magnetic fields parallel and perpendicular to the c-axis, respectively. Figure 2(b) shows the isothermal magnetization as a function of the magnetic field applied parallel to the c-axis. All the magnetization curves increase linearly with the magnetic field both in the antiferromagnetic state and paramagnetic state. No spin-flop transitions or ferromagnetic transitions were detected in the field range up to 7 T.

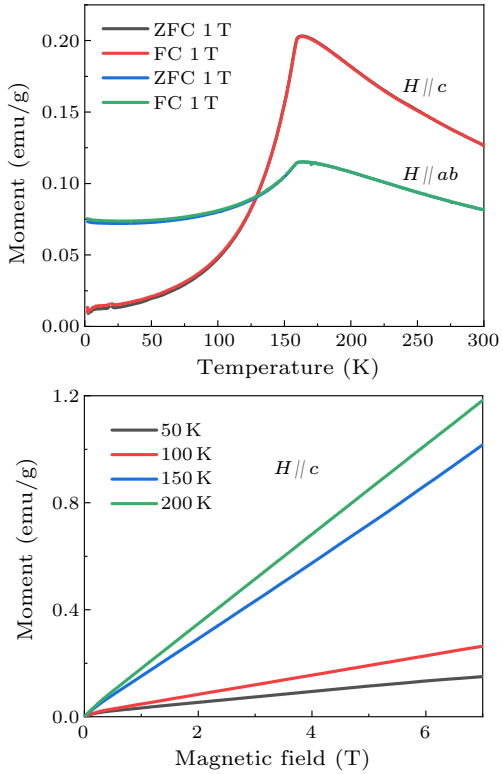


Fig. 2. (a) The temperature dependent magnetic susceptibility with the field applied both along the c-axis and the ab plane. (b) The isothermal magnetization as a function of the magnetic field applied along the c-axis.

Within the same field range where the antiferromagnetic state remains intact, the electrical transport properties of the compound were investigated. As illustrated in Fig. 3(a), the resistivity declines with cooling at relatively high temperatures and shows a slight upturn when approaching T_N, leaving a local maximum exactly at T_N, which is qualitatively similar to that of other magnetically intercalated TMDs.[9,12] It is speculated that the more rapid decrease of resistivity below T_N should be attributed to the weakened scattering between electrons and local spins due to the formation of spin ordering.[10] Figures 3(b) and 3(c) show the transverse magnetoresistance (MR) as a function of the magnetic field at various temperatures. Here, the MR is defined as

$$\mathrm{MR} = \frac{\rho(H) - \rho(0)}{\rho(0)}, \tag{2}$$

where $\rho(H)$ is the magnetic field dependent resistivity measured with H perpendicular to the current. It is shown that the MR is positive in the antiferromagnetic state and gradually evolves into negative values as the temperature elevates near T_N. The magnitude of the positive MR exhibits a maximum of only 0.5%, and the negative MR reaches a maximum of only -0.1%. In addition, the magnitudes of the positive MR are almost identical in both magnetic field directions, while the negative MR is severely suppressed with the applied field perpendicular to the c-axis. Yamada *et al.*[18,19] has calculated the MR of antiferromagnetic metals by taking the electron–spin scattering induced by a moderate s–d interaction into account. According to their calculations, though the magnetic field parallel to the easy axis introduces opposite energy shifts to the magnons of the two sublattices that constitute the antiferromagnetic lattice, respectively, the total number of excited magnons always increases with the field as long as the field is not strong enough to induce a spin-flop transition. As a consequence, the increased magnons give rise to more frequent scattering of electrons and lead to the positive MR. In regard to the circumstance where the field is perpendicular to the easy axis, the antiferromagnetic metal should also exhibit a positive MR if the influence of the optical mode is negligible, which would be proven to be valid for the title compound in later discussions. In both directions, the positive MR could increase quadratically with regard to the field in particular cases. While in the paramagnetic states, the external field increases the effective field imposing on local spins and suppresses the spin fluctuation, and a negative MR emerges as a result.[20,21] It is concluded that the spin fluctuation suffers a weaker suppression when the field is applied parallel to the ab plane. In a nutshell, their predictions provide a qualitatively satisfactory interpretation of our data. A previous ARPES research reported the absence of the band folding originating from antiferromagnetism in $Fe_{0.25}NbSe_2$, which indicates the weak coupling between electrons and local Fe moments.[22] In the temperature range from 2 K to 250 K, the Hall resistivity features a linear relationship with the field, accompanied by a sign reversal of slopes at around 120 K, which indicates a multi-band nature. In spite of the simultaneous contribution of electrons and holes, the carrier concentration n is derived straight from the slope considering that the curvature in Hall signals characterized by the two-carrier model is negligible in our measurements. As shown in the inset of Fig. 3(d), holes and electrons dominate at the low-temperature range and high-temperature range, respectively. Meanwhile, n_e shows a local minimum at T_N, and n_h decreases monotonically with cooling. It is noteworthy that the carrier concentration of the title compound reaches 7×10^{21} cm^{-3} at 100 K, which is moderately smaller than that of pristine $NbSe_2$ at the same temperature.[23] The decreased hole density upon intercalation plausibly results from the shrinkage of hole pocket owing to the upward shift of Fermi level and rigidity of pristine bands according to ARPES results.[22]

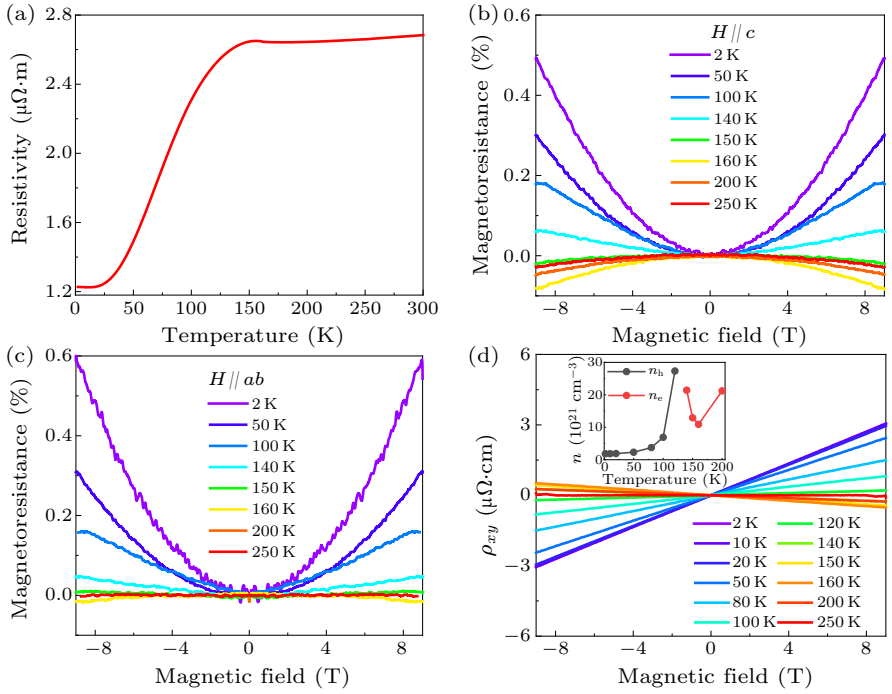


Fig. 3. (a) Temperature dependence of the longitudinal resistivity under zero magnetic field. The magnetic field dependence of the magnetoresistance with the field applied along (b) the *c*-axis and (c) the *ab* plane. (d) The magnetic field dependence of the Hall resistivity under different temperatures, the inset shows the carrier densities as a function of temperatures.

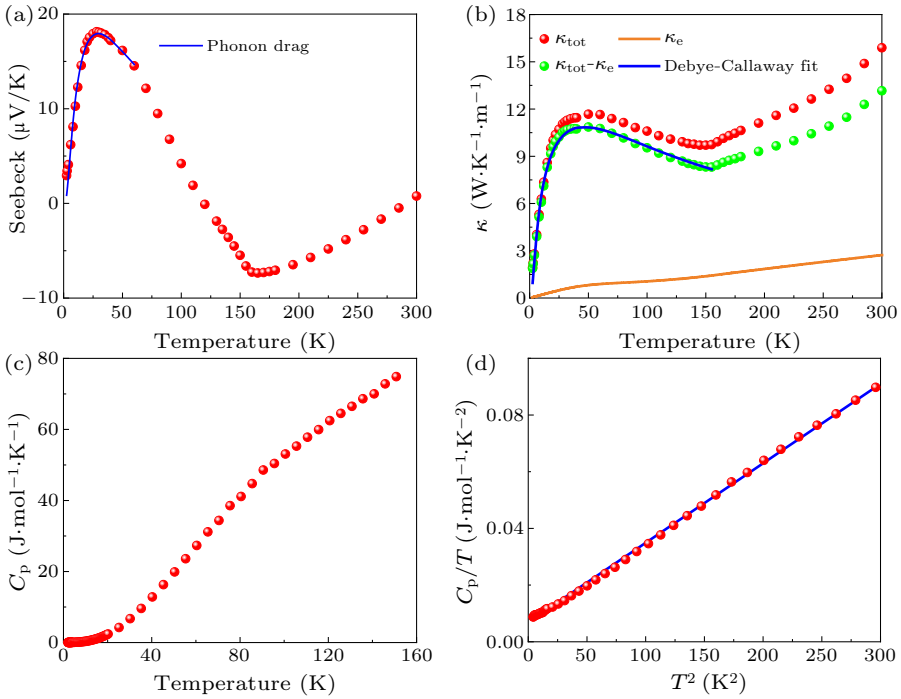


Fig. 4. (a) The red balls represent the Seebeck coefficient S at different temperatures and the blue solid line represents the phonon drag effect fit to the low-temperature part of S. (b) The temperature dependence of thermal conductivities, where red balls and green balls represent the total thermal conductivity and lattice thermal conductivity, respectively. The orange line and the blue line stand for the electron thermal conductivity calculated from the resistivity and the Debye–Callaway fit to the lattice thermal conductivity, respectively. (c) The temperature dependence of the specific heat C_p. (d) The plot of C_p/T versus T^2, and the blue solid line represent the fit based on the Debye model.

At last, in pursuit of a further comprehension of the interactions between quasiparticles in this compound, we carried out thermoelectric measurements on the single crystal samples. Figure 4(a) shows the Seebeck coefficient S as a function of the temperature. At relatively high temperatures, the negative S grows larger in magnitude with decreasing temperatures and forms a dip at T_N. With further cooling, S gradually becomes positive and shapes like a hump at relatively low temperatures, reaching a relatively large value of 18 μV/K at the summit. The sign reversal behavior of S is highly consistent with that of the Hall measurements. The hump-like feature of S at around 28 K is readily reminiscent of the phonon drag ef-

fect, signaled by a peak at the temperature which is a fraction of Debye temperature Θ_D. The temperature gradient in a solid will generate an inhomogeneous population of phonons, making the charge carriers that travel along the temperature gradient in opposite directions experience inequal scattering rates. Consequently, a spontaneous electric field will be induced in order to compensate the charge imbalance, which renders the so-called phonon drag contribution to S. A formula describing the phonon drag contribution to S was employed to fit the low temperature part of S

$$S_p = \frac{3k_B}{e}\left(\frac{T}{\theta}\right)^3 \int_0^{\frac{\theta}{T}} \frac{x^4 e^{-x} dx}{(1+e^{-x})^2\left(1+\frac{T}{\Phi}\right)^3 x^3}, \tag{3}$$

where Φ stands for the ratio of phonon–electron and electron–phonon scattering cross sections.[24] It is shown that the hump-like feature can be well fitted by this formula. In view of the antiferromagnetism in this compound, the possibility of magnon drag must be inspected. According to the previously reported results in elemental samples Fe, Co and Ni, the magnon drag contribution approximately follows a power law behavior of $S_m \propto T^{\frac{3}{2}}$ at low temperatures,[25] which is obviously inconsistent with the asymptotic T^3 behavior of the title compound. In addition, the magnetic field response of S is hardly detectable (not shown here), which further excludes the influence of magnons. As shown in Fig. 4(b), the thermal conductivity κ_{tot} declines monotonously with decreasing temperature until reaching T_N and forms a broad hump in the low-temperature range. The electron thermal conductivity κ_e was calculated by the Wiedemann–Franz law,[26] and the lattice thermal conductivity κ_L was obtained by subtracting κ_e from the total thermal conductivity κ_{tot}. The decreasing κ_L above T_N should be attributed to the scattering of phonons resulting from the strong spin fluctuation before the antiferromagnetically ordered state building up.[27] By combing sorts of scattering processes, a phenomenological theory for κ_L has been developed,[28–31] which states that scatterings related to crystalline boundaries, point impurities and phonon–phonon interactions successively dominate as the temperature gradually increases from low temperatures to high temperatures. Moreover, the asymptotic behaviors of κ_L at low-temperature and high-temperature limiting cases are proportional to T^3 and T^{-1}, respectively, leaving a maximum at the intermediate region. For the purpose of investigating the contributions of different scattering processes to κ_L, the Debye–Callaway model was employed to fit κ_L

$$\kappa_L = \frac{k_B}{2\pi^2 v}\left(\frac{k_B T}{\hbar}\right)^3 \int_0^{\frac{\theta_D}{T}} \frac{x^4 e^x dx}{\tau_c^{-1}(e^x-1)^2}, \tag{4}$$

where v is the average sound velocity, τ_c is the phonon scattering relaxation time and the dimensionless variable $x = \frac{\hbar\omega}{k_B T}$. Here, we consider a combination of grain boundary scattering, point impurity scattering, Umklapp scattering and resonance scattering and thus τ_c can be written as the following expression:

$$\tau_c^{-1} = \frac{v}{L} + A\omega^4 + B\omega^2 T e^{-\frac{\theta_D}{3T}} + \frac{C\omega^2}{(\omega_0^2-\omega^2)^2}, \tag{5}$$

where L is the grain boundary size, ω is the phonon frequency, ω_0 is the resonance frequency and A, B, C are fitting parameters. In comparison to the fitting results of quasi-one dimensional material KMn_6Bi_5[24] and heavy-fermion compound $YbCo_2Zn_{20}$,[32] the coefficient C of the title compound, which quantifies the strength of resonance scattering, is three orders of magnitudes smaller than that of them. Generally, the weakly bonded atoms reside in the voids of cage-like structures usually act as heavy rattler atoms that give rise to low-frequency optical phonons interacting with heat carrying acoustical phonons.[33–36] Therefore, it is asserted that the intercalated iron atoms are restricted tightly in the van der Waals gap of the title compound possibly owing to the formation of superlattices. For the purpose of further excluding the contribution of low-frequency optical phonons, the specific heat C_p as a function of temperatures at ambient pressure was measured. As shown in Fig. 4(d), the specific heat at low temperatures can be well fitted by the Debye model $C_p/T = \gamma + \beta T^2$, yielding an electronic specific heat coefficient γ of 6.88 mJ/mol·K^{-2} and a phonon specific heat coefficient β of 0.28 mJ/mol·K^{-4}. In comparison to γ of about 17 mJ/mol·K^{-2} of pristine $NbSe_2$, the diminished γ after intercalation might be attributed to the decrease of density of states at Fermi level, which has been detected previously in other transition metal intercalated $NbSe_2$ samples.[37,38] The fact that C_p at low temperatures can be well described by the Debye model without considering any Einstein modes indicates the negligible contribution of optical phonons.

4. Conclusions

In conclusion, the intercalation of Fe converts the pristine superconductor to an antiferromagnet, which exhibits a positive MR in the antiferromagnetic state and a negative MR in the paramagnetic state. And the sign reversal of MR is ascribed to the alternate dominance of increased magnons and suppressed spin fluctuations. The fact that the MR behaviors of the title compound strictly stay in line with the analytical calculations based on the perturbation of s–d interaction indicates the prominent role of scattering between local spins and electrons. The sign reversal of Hall and Seebeck signals indicates a multi-band structure. The negligible contribution of optical phonons is confirmed by the thermal conductivity and specific heat measurements. It is speculated that the intercalated Fe atoms are tightly bonded due to the formation

of superlattices. Therefore, an intercalation of lower concentrations at which the Fe atoms exhibit a random occupancy might reduce the lattice thermal conductivity and enhance the thermoelectric performance. On the other hand, if the Fe intercalation was maximized so that a well-developed superlattice comes into existence, the Dzyaloshinskii–Moriya interaction can probably be enhanced and lead to nontrivial spin textures. Consequently, various exotic phenomena might emerge which result from the interaction between spin textures and electrons. A more comprehensive research that includes samples with wide intercalation ranges is promising to reveal an insightful property evolution.

Acknowledgements

Project supported by the National Natural Science Foundation of China (Grant No. 12274440), the National Key R&D Program of China (Grant No. 2022YFA1403903), the Strategic Priority Research Program (B) of the Chinese Academy of Sciences (Grant No. XDB33010100), and the Fund of the Synergetic Extreme Condition User Facility (SECUF).

References

[1] Manzeli S, Ovchinnikov D, Pasquier D, Yazyev O V and Kis A 2017 *Nat. Rev. Mater.* **2** 17033
[2] Li D, Zhang X, He W, Peng Y and Xiang G 2023 *Sci. China Mater.* **67** 279
[3] Fang H, Lyu M, Su H, Yuan J, Li Y, Xu L, Liu S, Wei L, Liu X, Yang H, Yao Q, Wang M, Guo Y, Shi W, Chen Y, Liu E and Liu Z 2023 *Sci. China Mater.* **66** 2032
[4] Cheng Q, Xian G, Huang Y, Guo H, Pan L, Zhou H, Wang J, Lv S, Shen C, Lin X, Chen H, Li Y, Yang H and Gao H J 2023 *Sci. China Mater.* **66** 2393
[5] Dai C, He P, Luo L, Zhan P, Guan B and Zheng J 2023 *Sci. China Mater.* **66** 859
[6] Morosan E, Zandbergen H W, Dennis B S, Bos J W G, Onose Y, Klimczuk T, Ramirez A P, Ong N P and Cava R J 2006 *Nat. Phys.* **2** 544
[7] Bhatt R, Bhattacharya S, Patel M, Basu R, Singh A, Sürger C, Navaneethan M, Hayakawa Y, Aswal D K and Gupta S K 2013 *J. Appl. Phys.* **114** 114509
[8] Checkelsky J G, Lee M, Morosan E, Cava R J and Ong N P 2008 *Phys. Rev. B* **77** 014433
[9] Chen C W, Chikara S, Zapf V S and Morosan E 2016 *Phys. Rev. B* **94** 054406
[10] Polesya S, Mankovsky S, Ebert H, Naumov P G, Elghazali M A, Schnelle W, Medvedev S, Mangelsen S and Bensch W 2020 *Phys. Rev. B* **102** 174423
[11] Wang Z, Peng X, Zhang S, Su Y, Lai S, Zhou X, Wu C, Zhou T, Wang H, Yang J, Chen B, Zhai H, Wu Q, Du J, Jiao Z and Fang M 2024 *Chin. Phys. B* **33** 037301
[12] Liu P, Zhu H, Wu Q, Lu Y and Pu Y 2022 *Appl. Phys. Lett.* **121** 081901
[13] Ham W S, Pradipto A M, Yakushiji K, Kim K, Rhim S H, Nakamura K, Shiota Y, Kim S and Ono T 2021 *npj Comput. Mater.* **7** 129
[14] Zheng G, Wang M, Zhu X, Tan C, Wang J, Albarakati S, Aloufi N, Algarni M, Farrar L, Wu M, Yao Y, Tian M, Zhou J and Wang L 2021 *Nat. Commun.* **12** 3639
[15] Togawa Y, Kousaka Y, Nishihara S, Inoue K, Akimitsu J, Ovchinnikov A S and Kishine J 2013 *Phys. Rev. Lett.* **111** 197204
[16] Naik S, Pradhan A, Mishra A and Samal S L 2022 *J. Phys. Chem. C* **126** 13762
[17] Mugiraneza S and Hallas A M 2022 *Commun. Phys* **5** 95
[18] Yamada H and Takada S 1973 *J. Phys. Soc. Jpn.* **34** 51
[19] Yamada H and Takada S 1973 *Prog. Theor. Phys.* **49** 1401
[20] Negishi H, Yamada H, Yuri K, Sasaki M and Inoue M 1997 *Phys. Rev. B* **56** 11144
[21] Yamada H and Takada S 1972 *Prog. Theor. Phys.* **48** 1828
[22] Koh Y, Cho S, Lee J, Yang L X, Zhang Y, He C, Chen F, Feng D L, Arita M, Shimada K, Namatame H, Taniguchi M and Kim C 2013 *Jpn. J. Appl. Phys.* **52** 10MC15
[23] Li L J, Xu Z A, Shen J Q, Qiu L M and Gan Z H 2005 *J. Phys.: Condens. Matter* **17** 493
[24] Dong Q X, Huang Y F, Zhang L B, Bai J L, Cheng J W, Liu Q Y, Liu P Y, Li C D, Xiang J S, Wang J F, Ruan B B, Ren Z A, Sun P J and Chen G F 2023 *Appl. Phys. Lett.* **122** 094104
[25] Watzman S J, Duine R A, Tserkovnyak Y, Boona S R, Jin H, Prakash A, Zheng Y and Heremans J P 2016 *Phys. Rev. B* **94** 144407
[26] Chester G V and Thellung A 1961 *Proc. Phys. Soc.* **77** 1005
[27] Vasil'ev A N, Pryadun V V, Khomskii D I, Dhalenne G, Revcolevschi A, Isobe M and Ueda Y 1998 *Phys. Rev. Lett.* **81** 1949
[28] Callaway J and Von Baeyer H C 1960 *Phys. Rev.* **120** 1149
[29] Pohl R O 1962 *Phys. Rev. Lett.* **8** 481
[30] Callaway J 1959 *Phys. Rev.* **113** 1046
[31] Agrawal B K and Verma G S 1962 *Phys. Rev.* **126** 24
[32] Wei K, Neu J N, Lai Y, Chen K W, Hobbis D, Nolas G S, Graf D E, Siegrist T and Baumbach R E 2019 *Sci. Adv.* **5** eaaw6183
[33] Kovalsky A, Wang L, Marek G T, Burda C and Dyck J S 2017 *J. Phys. Chem. C* **121** 3228
[34] Dutta M, Das A and Biswas K 2024 *Inorg. Chem.* **63** 20068
[35] Qiu W, Xi L, Wei P, Ke X, Yang J and Zhang W 2014 *Proc. Natl. Acad. Sci. USA* **111** 15031
[36] Xie H, Su X, Zhang X, Hao S, Bailey T P, Stoumpos C C, Douvalis A P, Hu X, Wolverton C, Dravid V P, Uher C, Tang X and Kanatzidis M G 2019 *J. Am. Chem. Soc.* **141** 10905
[37] Luo H, Strychalska-Nowak J, Li J, Tao J, Klimczuk T and Cava R J 2017 *Chem. Mater.* **29** 3704
[38] Zhou M, Shi Y, Gu Y, Yi J, Chen L, Yang Q, Ruan B, Chen G and Ren Z 2024 *J. Alloys Compd.* **991** 174502